

A FACE-BASED SMOOTHED FINITE ELEMENT METHOD FOR HYPERELASTIC MODELS AND TISSUE GROWTH

MINH TUẤN DƯƠNG^{*,†} AND MANFRED STAAT^{*}

^{*} Aachen University of Applied Sciences Heinrich-Mußmann-Str. 1, 52428 Jülich, Germany
e-mail: {duong, m.staat}@fh-aachen.de - Web page www.fh-aachen.de

[†] Hanoi University of Science and Technology, No.1 Dai Co Viet Road, Hanoi, Vietnam
e-mail: tuan.duongminh@hust.vn - Web page www.hust.edu.vn

Key words: SFEM, FS-FEM, FEM, Hyperelastic Models, Nonlinear Problems.

Abstract. This paper presents a Face-based Smoothed Finite Element Method (FS-FEM) using the 4-node tetrahedral elements (T4) (FS-FEM-T4) applied to nonlinear problems. The FS-FEM can overcome and improve some existing problems which the standard Finite Element Method using the T4 (FEM-T4) often faces, such as the well-known overly stiff behavior, poor stress solution, and volumetric effects. The principal idea of the FS-FEM is to formulate a strain field as a spatial average of the standard strain measure. In the field of biomechanics, the FS-FEM is still relative new. We have implemented the FS-FEM into the open source software *Code_Aster* for large scale biomedical applications. Numerical results of the FS-FEM for linear and nonlinear problems show clearly its advantages in improving accuracy particularly for the distorted meshes. A combination of the FS-FEM with the growth models performed exhibits clearly good performances.

1 INTRODUCTION

The 4-node tetrahedral element can automatically be created according to the Delaunay techniques, which are capable of producing a tetrahedral mesh for any geometry, however complicated, such as human body and organs. If the FEM-T4 is used, then there are still crucial shortcomings of the method for problems of solid mechanics existing such as the well-known overly stiff behavior, poor stress solution, and volumetric locking in nearly incompressible cases.

In order to overcome these disadvantages of using the T4, some new finite elements were proposed. The mixed formulations (mixed-enhanced elements) can avoid such difficulties [1, 2]. Average nodal pressure for tetrahedral elements was proposed by [3] and applied with extensions for better handling of multiple material surfaces to surgical simulation [4]. Nevertheless, the volumetric locking can be avoided or significantly reduced but the performances such as accuracy are still not fully improved.

Based on the work of Chen et al. [5] on stabilized conforming nodal integration Liu et al. [6] introduced the Smoothed Finite Element Method (SFEM). The principal idea of the SFEM is to formulate a strain field as a spatial average of the standard strain measure. Specifically, four different smoothing domains created based on cells (elements), nodes, edges, and faces are used to establish four different SFEM models: Cell-based SFEM (CS-FEM), Node-based SFEM(NS-FEM), Edge-based SFEM(ES-FEM), and Face-based SFEM(FS-FEM). Each of the four SFEM models has different advantages and disadvantages. For heat transfer problems, the four-noded tetrahedral element was adopted [7]. The FS-FEM was used for 3D visco-elastoplastic problems [8] and employed for nonlinear problems [9]. In biomechanics or biomedical applications, there is very few research using the SFEM for biological soft tissues. The ES-FEM was applied to plate problems (soft tissue membrane) [10]. Up to date, the FS-FEM was immersed into a complex FEM model for fluid-structure interaction simulation of aortic valves [11]. Therefore, the SFEM is adequate to be chosen for applications of biological soft tissue.

In this paper, the FS-FEM-T4 is presented in detail for problems raising in biomechanics and biomedical engineering. A number of numerical results is presented to demonstrate the efficiency and properties of the model. Moreover, a combination of the growth models and the FS-FEM is made.

2 FACE-BASED SMOOTHING DOMAIN CREATION

A 3D domain Ω is discretized with n_e tetrahedral elements and n_n nodes such that $\Omega = \cup_{m=1}^{n_e} \Omega_m^e$ and $\Omega_i^e \cap \Omega_j^e \neq \emptyset, i \neq j$. The T4 element mesh has a total of $n_f = 4$ faces. The virtual displacements $\mathbf{u}^h(\mathbf{x})$, and the compatible strains $\boldsymbol{\epsilon} = \nabla_s \mathbf{u}$ (∇_s is the symmetric part of displacement gradient) within any element can be computed as

$$\mathbf{u}^h(\mathbf{x}) = \sum_I^{n_d} \mathbf{N}_I \mathbf{u}_I = \mathbf{N}_I \mathbf{u}_I, \quad \boldsymbol{\epsilon}^h(\mathbf{x}) = \sum_I^{n_d} \mathbf{B}_I \mathbf{u}_I = \mathbf{B}_I \mathbf{u}_I, \quad (1)$$

where n_d is the number of nodal variables of the element, \mathbf{N}_I is the linear shape function matrix and \mathbf{B}_I is the standard displacement gradient matrix of the node I .

Based on the faces of elements, the smoothing strain technique [5] is applied to create smoothing domains, such that $\Omega = \cup_{k=1}^{n_f} \Omega^k$ and $\Omega_i^k \cap \Omega_j^k \neq \emptyset, i \neq j$. The smoothing domain Ω^k associated with the face k is created by simply connecting three nodes of the face to the centers of the adjacent elements as shown in Figure 1. The smoothed strain on the smoothing domain Ω^k associated with the face k is calculated as

$$\bar{\boldsymbol{\epsilon}} = \int_{\Omega^k} \boldsymbol{\epsilon}(\mathbf{x}) \Phi_k(\mathbf{x}) dV = \int_{\Omega^k} \nabla_s \mathbf{u}(\mathbf{x}) \Phi_k(\mathbf{x}) dV, \quad (2)$$

where $\Phi_k(\mathbf{x})$ is a given smoothing function which satisfies at least the unity property as

$$\int_{\Omega^k} \Phi_k(\mathbf{x}) dV = 1. \quad (3)$$

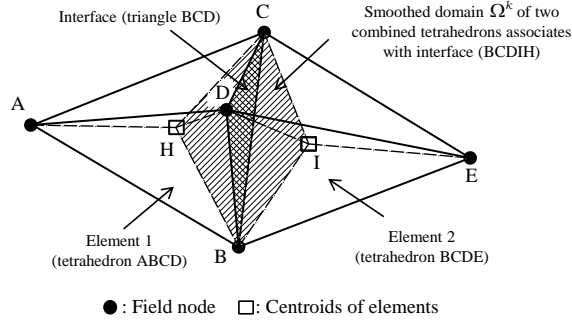


Figure 1: Smoothing domain created on interface of two neighboring elements.

The locally constant smoothing function is used as follows

$$\Phi_k(\mathbf{x}) = \begin{cases} \frac{1}{V^k}, & \mathbf{x} \in \Omega^k \\ 0, & \mathbf{x} \notin \Omega^k, \end{cases} \quad (4)$$

where the V^k is the volume of the smoothing domain Ω^k and is evaluated as

$$V^k = \int_{\Omega^k} dV = \frac{1}{4} \sum_{m=1}^{n_{sb}^k} V_{(m)}^e, \quad (5)$$

where n_{sb}^k is the number of subsmoothing domains and is also exactly the number of elements around the faces k ($n_{sb}^k = 1$ for boundary and $n_{sb}^k = 2$ for inner faces) and $V_{(m)}^e$ is the volume of the m^{th} element around the face k .

The trial function $\mathbf{u}^h(\mathbf{x})$ in the FS-FEM is computed as the same as in (1) of the FEM, which leads to the nodal force vector in the FS-FEM calculated in the similar way as in the FEM. Substituting (1) into (2), the smoothed strain on the domain Ω^k associated with face k can be written in the following matrix form of nodal displacements:

$$\bar{\boldsymbol{\epsilon}} = \sum_{I \in n_n^k} \bar{\mathbf{B}}_I(\mathbf{x}_k) \mathbf{u}_I, \quad (6)$$

where n_n^k is the total number of nodes of elements containing the common face k ($n_n^k = 4$ for boundary faces and $n_n^k = 5$ for inner faces) and $\bar{\mathbf{B}}_I(\mathbf{x}_k)$, which is termed the smoothed strain matrix on the domain Ω^k .

Thanks to the use of the tetrahedral elements with the linear shape functions, the entries of the matrix \mathbf{B}^e are constants over each element, and hence the smoothed strain-displacement matrix $\bar{\mathbf{B}}_I$ on the domain Ω^k is numerically computed by an local assembly process as

$$\bar{\mathbf{B}}_I = \frac{1}{V^k} \sum_{m=1}^{n_e^k} \frac{1}{4} V_{(m)}^e \mathbf{B}_{(m)}^e, \quad (7)$$

where $\mathbf{B}_{(m)}^e$ is the strain-displacement matrix of the m^{th} element attached to the face k .

If the divergence theorem is applied, the smoothed strain matrix $\bar{\mathbf{B}}_I(\mathbf{x}_k)$ can generally be evaluated on the domain Ω^k in an alternative way by

$$\bar{\mathbf{B}}_I(\mathbf{x}_k) = \frac{1}{V^k} \int_{\Gamma^k} \mathbf{n}^{(k)}(\mathbf{x}) \mathbf{N}_I(\mathbf{x}) dS = \begin{bmatrix} \bar{B}_{I1}(\mathbf{x}_k) & 0 & 0 \\ 0 & \bar{B}_{I2}(\mathbf{x}_k) & 0 \\ 0 & 0 & \bar{B}_{I3}(\mathbf{x}_k) \\ \bar{B}_{I2}(\mathbf{x}_k) & \bar{B}_{I1}(\mathbf{x}_k) & 0 \\ 0 & \bar{B}_{I3}(\mathbf{x}_k) & \bar{B}_{I2}(\mathbf{x}_k) \\ \bar{B}_{I3}(\mathbf{x}_k) & 0 & \bar{B}_{I1}(\mathbf{x}_k) \end{bmatrix}, \quad (8)$$

where Γ^k is the boundary of the smoothing domain Ω^k with the volume V^k , and $\mathbf{n}^{(k)}(\mathbf{x})$ is the outward normal vector matrix on the boundary Γ^k and has the form (based on Voigt's notation)

$$\mathbf{n}^{(k)}(\mathbf{x}) = \begin{bmatrix} n_1^{(k)} & 0 & 0 \\ 0 & n_2^{(k)} & 0 \\ 0 & 0 & n_3^{(k)} \\ n_2^{(k)} & n_1^{(k)} & 0 \\ 0 & n_3^{(k)} & n_2^{(k)} \\ n_3^{(k)} & 0 & n_1^{(k)} \end{bmatrix}. \quad (9)$$

Theoretically, the FS-FEM also works for other types of elements, as long as a continuous displacement field on the smoothing domain surface can be created.

3 FS-FEM FOR NONLINEAR ANALYSIS

In this section, the total Lagrangian formulation for the FS-FEM based on the standard FEM is described for physically and geometrically nonlinear problems in solid mechanics. Consider a body, which is subjected to a body force \mathbf{b}_0 on the reference configuration Ω_0 and the external traction \mathbf{T} on the boundary Γ_0 . By using $\delta \mathbf{u}^h(\mathbf{x}) = \sum_I^{n_d} \mathbf{N}_I \delta \mathbf{u}_I$ the general variation equation in the nonlinear FEM for the total virtual work can be evaluated as

$$\delta \Pi(\mathbf{u}, \delta \mathbf{u}) = \delta \mathbf{u}^T \cdot \left(\int_{\Omega_0} \mathbf{B}^T \mathbf{S} dV - \int_{\Omega_0} \mathbf{N}^T \mathbf{b}_0 dV - \int_{\Gamma_0} \mathbf{N}^T \mathbf{T} dS \right) = 0. \quad (10)$$

By invoking the arbitrariness of virtual nodal displacements and using load increments with a load factor λ , the FEM-T4 formulation based on the total Lagrange formulation [12] and the discrete system of equations can be expressed as follows

$$\mathbf{K}_t \Delta \mathbf{u} = (\mathbf{K}_M + \mathbf{K}_G) \Delta \mathbf{u} = \mathbf{F}_{int}(\mathbf{u}) - \lambda \mathbf{F}_{ext}(\mathbf{u}), \quad (11)$$

where the internal force vector and the external force vector can be introduced from the first integral of the principle of virtual work as

$$\mathbf{F}_{int} = \int_{\Omega_0} \mathbf{B}^T \mathbf{S} dV, \quad \mathbf{F}_{ext} = \int_{\Omega_0} \mathbf{N}^T \mathbf{b}_0 dV + \int_{\Gamma_0} \mathbf{N}^T \mathbf{T} dS. \quad (12)$$

Based on the FEM, the FS-FEM can be expressed as follows. All quantities need to be smoothed and computed on smoothing domains. The smoothed material stiffness matrix for the linearized portion can be written as

$$\bar{\mathbf{K}}_M = \sum_{k=1}^{n_f} \bar{\mathbf{K}}_M^k, \quad \bar{\mathbf{K}}_M^k = \int_{\Omega^k} (\bar{\mathbf{B}}_M^k)^T \mathbb{D} \bar{\mathbf{B}}_M^k dV = (\bar{\mathbf{B}}_M^k)^T \mathbb{D} \bar{\mathbf{B}}_M^k V^k, \quad (13)$$

where $\bar{\mathbf{K}}_M^k$ is the smoothed material stiffness on the smoothing domain Ω^k with its volume V^k associated with the face k , and \mathbb{D} is the constitutive matrix. $\bar{\mathbf{B}}_M^k$ is the smoothed strain-displacement matrix on the smoothing domain Ω^k calculated as

$$\bar{\mathbf{B}}_M^k = \frac{1}{V^k} \sum_{m=1}^{n_k^e} \frac{1}{4} V_{(m)}^e \mathbf{B}_{(m)}^e, \quad (14)$$

in which the $\mathbf{B}_{(m)}^e$ of the m^{th} element is

$$\mathbf{B}_{(m)}^e = [\mathbf{B}_1 \quad \mathbf{B}_2 \quad \mathbf{B}_3 \quad \mathbf{B}_4], \quad (15)$$

where

$$\mathbf{B}_I = \begin{bmatrix} F_{11}N_{I,1} & F_{21}N_{I,1} & F_{31}N_{I,1} \\ F_{12}N_{I,2} & F_{22}N_{I,2} & F_{32}N_{I,2} \\ F_{13}N_{I,3} & F_{23}N_{I,3} & F_{33}N_{I,3} \\ F_{11}N_{I,2} + F_{12}N_{I,1} & F_{21}N_{I,2} + F_{22}N_{I,1} & F_{31}N_{I,2} + F_{32}N_{I,1} \\ F_{12}N_{I,3} + F_{13}N_{I,2} & F_{22}N_{I,3} + F_{23}N_{I,2} & F_{32}N_{I,3} + F_{33}N_{I,2} \\ F_{11}N_{I,3} + F_{13}N_{I,1} & F_{21}N_{I,3} + F_{23}N_{I,1} & F_{31}N_{I,3} + F_{33}N_{I,1} \end{bmatrix} \quad (I = 1, 2, 3, 4), \quad (16)$$

in which, $N_{I,J} = \frac{\partial N_I}{\partial X_J}$ and the $F_{i,J}$ ($i, J = 1, 2, 3$) are the entries of the deformation gradient tensor \mathbf{F} of the element. The second term on the left hand side in (11) is the material stiffness matrix concerning the nonlinear constitutive relation and is evaluated as

$$\bar{\mathbf{K}}_G = \sum_{k=1}^{n_f} \bar{\mathbf{K}}_G^k = \sum_{k=1}^{n_f} (\bar{\mathbf{B}}_G^k)^T \bar{\mathbf{S}}_G \bar{\mathbf{B}}_G^k V^k, \quad (17)$$

where matrix $\bar{\mathbf{B}}_G^k$ results from the geometrical nonlinearity of the linearization of variation of the Green strain \mathbf{E} . It is written in a form as

$$\bar{\mathbf{B}}_G^k = \frac{1}{V^k} \sum_{m=1}^{n_k^e} \frac{1}{4} V_{(m)}^e \mathbf{B}_{G(m)}^e. \quad (18)$$

In the foregoing equation, matrix $\mathbf{B}_{G(m)}^e$ is for the m^{th} element, and is generally given by

$$\mathbf{B}_G^e = \begin{bmatrix} N_{1,1} & 0 & 0 & N_{2,1} & \dots & 0 \\ N_{1,2} & 0 & 0 & N_{2,2} & \dots & 0 \\ N_{1,3} & 0 & 0 & N_{2,3} & \dots & 0 \\ 0 & N_{1,1} & 0 & 0 & \dots & 0 \\ 0 & N_{1,2} & 0 & 0 & \dots & 0 \\ 0 & N_{1,3} & 0 & 0 & \dots & 0 \\ 0 & 0 & N_{1,1} & 0 & \dots & N_{4,1} \\ 0 & 0 & N_{1,2} & 0 & \dots & N_{4,2} \\ 0 & 0 & N_{1,3} & 0 & \dots & N_{4,3} \end{bmatrix}. \quad (19)$$

The stress matrix $\bar{\mathbf{S}}_G$ for the face-based smoothing domains is computed using

$$\bar{\mathbf{S}}_G = \frac{1}{V^k} \sum_{m=1}^{n_k^e} \frac{1}{4} V_{(m)}^e \mathbf{S}_{G(m)}^e, \quad (20)$$

where $\mathbf{S}_{G(m)}^e$, see [12], is the hyper-diagonal matrix of the second Piola-Kirchhoff stress components of the m^{th} element, generally defined as

$$\mathbf{S}_G^e = \begin{bmatrix} S_{11} & S_{12} & S_{13} & 0 & 0 & 0 & 0 & 0 & 0 \\ S_{21} & S_{22} & S_{23} & 0 & 0 & 0 & 0 & 0 & 0 \\ S_{31} & S_{32} & S_{33} & 0 & 0 & 0 & 0 & 0 & 0 \\ 0 & 0 & 0 & S_{11} & S_{12} & S_{13} & 0 & 0 & 0 \\ 0 & 0 & 0 & S_{21} & S_{22} & S_{23} & 0 & 0 & 0 \\ 0 & 0 & 0 & S_{31} & S_{32} & S_{33} & 0 & 0 & 0 \\ 0 & 0 & 0 & 0 & 0 & 0 & S_{11} & S_{12} & S_{13} \\ 0 & 0 & 0 & 0 & 0 & 0 & S_{21} & S_{22} & S_{23} \\ 0 & 0 & 0 & 0 & 0 & 0 & S_{31} & S_{32} & S_{33} \end{bmatrix}, \quad (21)$$

in which the entries S_{IJ} are derived from the second Piola-Kirchhoff stress tensor \mathbf{S}^e of the element attached to the face k . In fact, there are no additional DOFs in the FS-FEM, so the external force vector can be similarly evaluated as the one in standard FEM. However, the internal force vector is now calculated based on the stress on the smoothing domain (smoothed stress) and is represented as

$$\mathbf{F}_{int} = \sum_{k=1}^{n_f} \mathbf{f}_{int}^k = \sum_{k=1}^{n_f} (\bar{\mathbf{B}}^k)^T \bar{\mathbf{S}}^k V^k. \quad (22)$$

Alternative way to compute smoothed quantities

The convenient approach can be implemented into the open source programs by smoothing the deformation gradient tensor. The smoothed deformation gradient $\bar{\mathbf{F}}^k$ of the smoothing

Table 1: Fitted parameters for HSF and proposed models

Model	$\mu[kPa]$	$k_{1H}[kPa]$	k_{2H}	k_{4p}	$k_{5p}[kPa]$	$\alpha[^\circ]$
Model 6	22.7223	0.0057	189.1230	274.6185	666.5237	50.7875

domain V^k is obtained in terms of the smoothed strain matrix (for the linear part) and the nodal displacement by applying the divergence theorem

$$\begin{aligned}\bar{\mathbf{F}}^k &= \frac{1}{V^k} \int_{V^k} \left[\frac{\partial \mathbf{u}}{\partial \mathbf{X}} + \mathbf{I} \right] dV = \frac{1}{V^k} \int_{V^k} \frac{\partial \mathbf{u}}{\partial \mathbf{X}} dV + \mathbf{I}, \\ \bar{\mathbf{F}}^k &= \bar{\mathbf{B}}(\mathbf{x}_k) \mathbf{u} + \mathbf{I}.\end{aligned}\tag{23}$$

4 FS-FEM APPLIED TO ANISOTROPIC HYPERELASTIC MODELS

In this section, the suggested strain-energy function [13] dealing with the instability of the Holzapfel model [14] is used in numerical simulations by the FS-FEM and defined as

$$\begin{aligned}W &= \frac{\mu}{2}(I_1 - 3) + W_{ani}(\bar{I}_4, \bar{I}_6) + W_{inter}(\bar{I}_1, \bar{I}_8), \\ W_{ani}(I_4, I_6, J) &= \frac{k_{1H}}{2k_{2H}} \{ \exp[k_{2H}(I_4 - 1)^2] - 1 \} + \frac{k_{1H}}{2k_{2H}} \{ \exp[k_{2H}(I_6 - 1)^2] - 1 \}, \\ W_{inter}(\bar{I}_1, \bar{I}_8) &= \frac{k_{5p}}{4k_{4p}} \{ \exp[k_{4p}(\bar{I}_1 + \bar{I}_8 - 3 - (c^2 - s^2)^2)] - 1 \},\end{aligned}\tag{24}$$

where the material parameters: $k_{1H} \geq 0$ (dimension of a modulus); $k_{2H} > 0$ (dimensionless coefficient); invariants: $I_1 = \text{tr} \mathbf{C}$, $I_4 = \mathbf{a}_0 \cdot \mathbf{C} \mathbf{a}_0$ and $I_6 = \mathbf{g}_0 \cdot \mathbf{C} \mathbf{g}_0$; in which $\mathbf{a}_0 = [0 \ \cos(\alpha) \ \sin(\alpha)]^T$ and $\mathbf{g}_0 = [0 \ \cos(\alpha) \ -\sin(\alpha)]^T$, α is an angle between two fiber families of soft biological tissues, \mathbf{C} is the right Cauchy Green strain tensor, and μ is equivalent to the small strain shear modulus. The material constants are achieved by fitting the experimental data for the adventitia in [15], see Table 1.

4.1 A 3D rectangle plate and a 3D cubic cantilever beam

A 3D rectangle plate (dimension: $100 \times 100 \times 2$ [mm^3]) is subjected to a pressure $p = 0.3$ KPa on the lower face and its two side faces are fixed. The plate is discretized with distorted elements (aspect ratio $\beta \approx 20$), see Figure 2a. The mesh consists of 1647 T4 elements and 546 nodes. The neo-Hookean model is used with the shear modulus $\mu = 190.6$ KPa. The deflection of the interested point A is shown in Figure 2. It is clear that the FS-FEM-T4 improves significantly the distorted mesh and is even better than the FEM-T4 for the non-distorted mesh (the same set of nodes). Both FS-FEM-T4 curves are above (larger magnitudes) the ones of the FEM-T4 and are of course closer to the solutions which are achieved from employing higher order elements.

A 3D cubic cantilever beam with the dimension ($2 \times 10 \times 2$ [cm^3]) is depicted in Figure 3. The T4-mesh contains 3570 elements and 951 nodes, shown in Figure 3. The

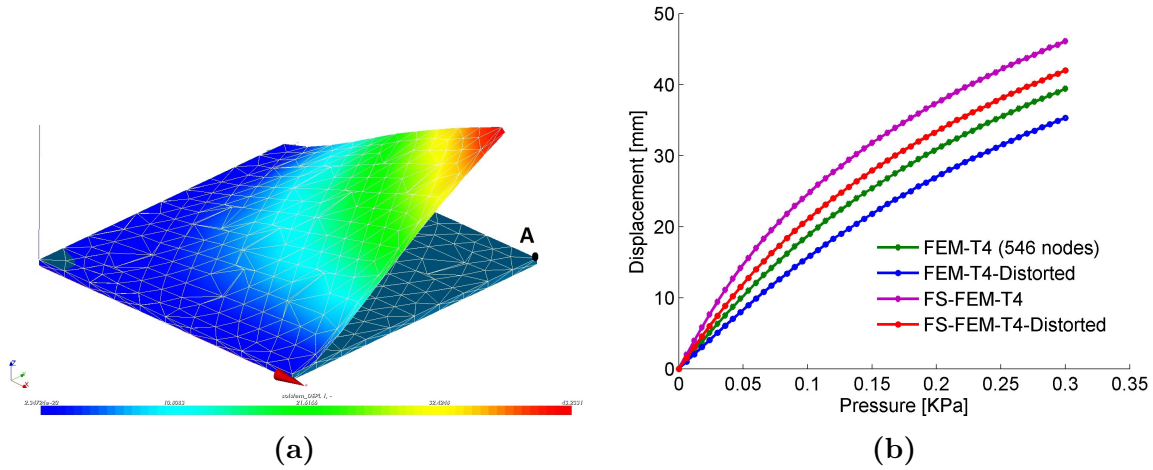


Figure 2: A 3D plate with a distorted mesh (a); displacement of the point A (b).

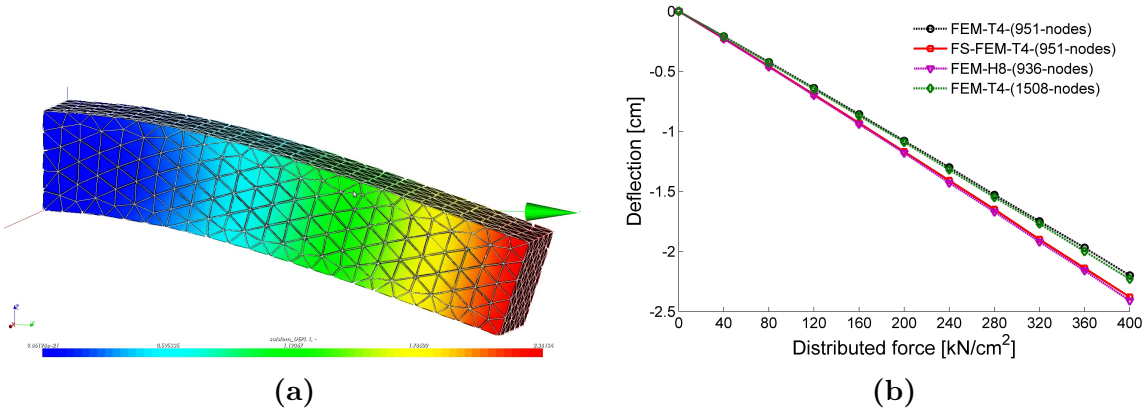


Figure 3: Deformed shape of the beam (a); tip deflection of the beam (b).

cantilever bar is subjected to a distributed force of 400 kN/cm^2 on the upper face. The material constants are presented in Table 1. The result of the FS-FEM-T4 is very close to the FEM-H8 with a similar number of nodes, see Figure 3. While the FS-FEM-T4 is much more accurate than the one of the standard FEM-T4 with the same mesh and even better than the FEM-T4 with a very finer mesh. Thus, the performance of the FS-FEM-T4 is relatively equivalent to the FEM-H8 when the same set of nodes is used. This exhibits the advantageous property of the FS-FEM as discussed before.

5 MODELING OF TISSUE GROWTH

Consider a body which grows by external stimulations such as loads (stress-induced growth). *The multiplicative decomposition of the deformation gradient* into its elastic part and the growth term is

$$\mathbf{F} = \mathbf{F}_e \cdot \mathbf{F}_g \quad \det(\mathbf{F}_g) \neq 1; \det(\mathbf{F}_e) = 1. \quad (25)$$

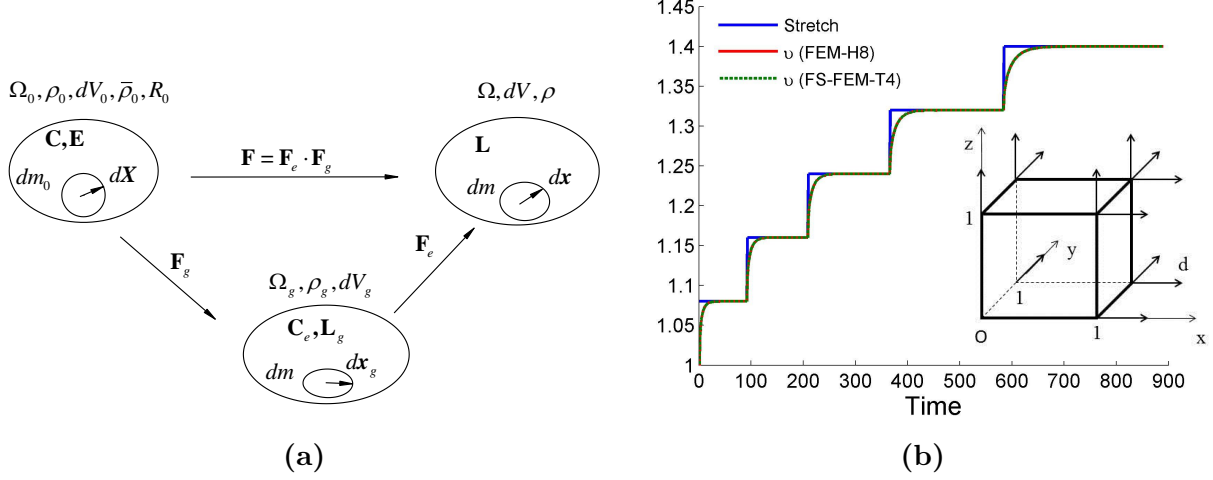


Figure 4: Multiplicative decomposition of \mathbf{F} (a); stretch and growth stretch ratio v (b).

$\det(\mathbf{F}_g) \neq 1$ since growth does not require volume preservation [16], see Figure 4a. The following expression for the growth part of the deformation gradient due to isotropic volume mass growth [17] in terms of a stretch ratio v is

$$\mathbf{F}_g = v\mathbf{I}, \quad (26)$$

Evolution equations for stretch ratio

For density preservation [18], in the simplest case the rate of the stretch ratio depends linearly on the trace of stress and the strain in the intermediate configuration, such that

$$\dot{v} = k_v(v) \text{tr}(\mathbf{S}_e \cdot \mathbf{C}_e). \quad (27)$$

where, \mathbf{C}_e and \mathbf{S}_e are the right Cauchy strain tensor and the second Piola-Kirchhoff stress tensor caused by the elastic deformation. To prevent an unlimited growth at an arbitrary non-zero state of stress, it is proposed that during the mass growth [17]

$$k_v(v) = k_{v_0}^+ \left(\frac{v^+ - v^-}{v^+ - 1} \right)^{m_v^+} \quad \text{for } \text{tr}(\mathbf{S}_e \cdot \mathbf{C}_e) > 0, \quad (28)$$

where $v^+ > 1$ is the limiting value of the growth stretch ratio v that can be attained by mass growth, and $k_{v_0}^+$ and m_v^+ are the material parameters. In the case of the mass resorption, the corresponding expression is

$$k_v(v) = k_{v_0}^- \left(\frac{v - v^-}{1 - v^-} \right)^{m_v^-} \quad \text{for } \text{tr}(\mathbf{S}_e \cdot \mathbf{C}_e) < 0. \quad (29)$$

The elasticity tensor in this case is evaluated as

$$\mathbb{C}_e = \mathbb{C} + \mathbb{C}_v \quad \text{in which} \quad \mathbb{C} = 2 \frac{\partial \mathbf{S}_e}{\partial \mathbf{C}_e} \quad \text{and} \quad \mathbb{C}_v = 2 \frac{\partial \mathbf{S}_e}{\partial v} \otimes \frac{\partial v}{\partial \mathbf{C}_e}. \quad (30)$$

Table 2: Material constants for growth simulation

Model	$\mu[kPa]$	$k_{1H}[kPa]$	k_{2H}	k_{4p}	$k_{5p}[kPa]$	$\alpha[^\circ]$
Model 6	1.272	1.0	1.912	27.462	1.0	50.78

Table 3: Growth constants

$k_{v,0}^+$	$k_{v,0}^-$	m_v^+	m_v^-	v^+	v^-	$\Delta t(time)$
0.8e-3	0.8e-3	2.5	3	2	0.5	1

The fourth order constitutive component caused by growth \mathbb{C}_v is not symmetric.

FS-FEM applied to the growth model: The implicit Euler backward scheme was adopted for solving these equations above for the increments of the growth stretch ratios in parallel with smoothing the growth tensor \mathbf{F}_g . Then, in each iteration of the Newton-Raphson loop for each smoothing domain, the growth stretch ratio is updated in the framework of the constitutive matrix as

$$v_{n+1} = v_n + \dot{v}\Delta t. \quad (31)$$

The constitutive matrix is therefore updated by the growth part and the elastic part.

5.1 Numerical test for growth-triaxial tension test of a cube

In this subsection, the FS-FEM-T4 is applied to the tissue growth in the triaxial tension test. The Poisson's ratio $\nu = 0.4$ or even $\nu = 0.3$ [18] was adopted. Consequently, the FS-FEM-T4 can fully adopted for growth simulation without regarding volumetric locking. The anisotropic material (24) is chosen with its parameters in Table 2 and the growth constants in Table 3. The intermediate configuration (growth one) is incompatible. Thus, loading can be applied to three directions. For five load increments of the monotonic loading, each of them has a value of 0.08, the stretch ratio of the isotropic growth is computed as shown in Figure 4b using the FEM-H8 and the FS-FEM-T4. Both methods result in the same solution. The stresses vanish in biological equilibrium what can be observed in the growth results, see Figure 5a. The grown cube has the volume $V = 2.744V_0$ in which V_0 is its initial volume. Furthermore, the limiting value for extension growth is $v^+ = 2$ and is still larger than the final principal prescribed stretch 0.4, see Figure 4b. Thus, the cube can grow further if it is stimulated with external loads until the stretch ratio reaches a value of 2. After this limiting value, if the cube is still subjected to external loading, then it induces corresponding stresses.

Even for the anisotropic materials used here, our results are qualitatively comparable with the ones using an isotropic hyperelastic model of the work of Himpel et al. [18].

6 CONCLUSIONS

The FS-FEM is first implemented into *Code_Aster* [19] for large scale biomedical applications. In the analysis of the 3D plate, the very important conclusion is that solutions

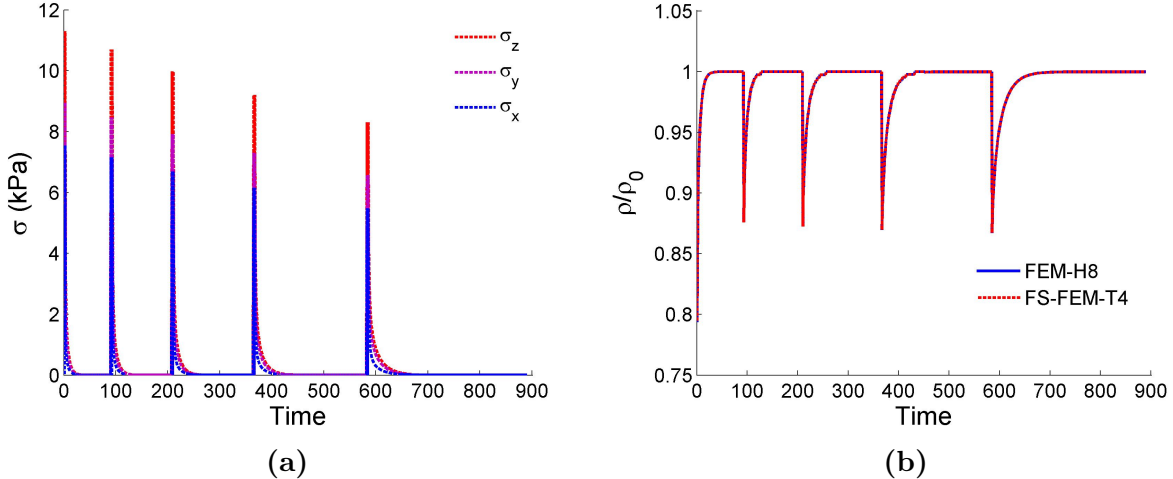


Figure 5: Stresses and density of the cube using the proposed model [13].

of the FS-FEM-T4 are less sensitive with the distortion of the meshes compared to those of the FEM-T4. In addition, the nonlinear case of solving the 3D cantilever beam with the anisotropic material model [13] can be considered the first application employing the FS-FEM for strong anisotropy (e.g. arteries). The FS-FEM solution has higher accuracy and its accuracy and convergence can be compatible to those of the standard FEM with 8-node hexahedral element (H8) (FEM-H8) using the same number of nodes. Through the growth simulation of the cube, the growth models [17] are first analyzed by the FS-FEM with expected performances. To this end, internal variables of the growth models are modified properly, the growth tensor is smoothed, and the implicit Euler integration is implemented. The FS-FEM not only brings about higher accuracy but relative insensitivity to volumetric locking if it is combined with the NS-FEM called a FS/NS-FEM model. This is a very promising trend for applying the FS-FEM in biomechanics in which soft tissues are typically incompressible materials. In conclusion, the FS-FEM brings about the advantageous properties and is hence capable of being fully applied to applications with lower computational cost such as virtual reality.

REFERENCES

- [1] Simo, J.C. and Rifai, M.S. A class of mixed assumed strain methods and the method of incompatible modes. *International Journal for Numerical Methods in Engineering*. (1990) **29**:1595-1638.
- [2] Taylor, R.L. A mixed-enhanced formulation tetrahedral finite elements. *International Journal for Numerical Methods in Engineering*. (2000) **47**:205-227.
- [3] Bonet, J. and Burton, A.J. A simple average nodal pressure tetrahedral element for incompressible and nearly incompressible dynamic explicit applications. *Communications in Numerical Methods in Engineering*. (1998) **14**:437-449.
- [4] Joldes, G.R., Wittek, A. and Miller K. Non-locking tetrahedral finite element for

- surgical simulation. *Commun. Numer. Meth. Engng.* (2009) **25**:827-836.
- [5] Chen, J.S., Wu, C.T., Yoon, S., You, Y. A stabilized conforming nodal integration for Galerkin mesh-free methods. *Int. J. Numer. Meth. Engng.* (2001) **50**:435-466.
- [6] Liu, G.R., Dai, K.Y. and Nguyen, T.T. A smoothed finite element method for mechanics problems. *Computational Mechanics.* (2007) **39**:859-877.
- [7] Xue, B.Y., Wu, S.C., Zhang, W.H. and Liu, G.R. A smoothed FEM (S-FEM) for heat transfer problems. *International Journal of Computational Methods.* (2013) **10**:01-14.
- [8] Nguyen-Thoi, T., Liu, G.R., Vu-Do, H.C. and Nguyen-Xuan, H. A face-based smoothed finite element method (FS-FEM) for visco-elastoplastic analyses of 3D solids using tetrahedral mesh. *Computer Methods in Applied Mechanics and Engineering.* (2009) **198**:3479-3498.
- [9] Nguyen-Thoi, T., Liu, G. R., Lam, K. Y. and Zhang, G. Y. A face-based smoothed finite element method (FS-FEM) for 3D linear and geometrically non-linear solid mechanics problems using 4-node tetrahedral elements. *Int. J. Numer. Meth. Engng.* (2008) **78**:324-353.
- [10] Frotscher, R. and Staat, M. Application of an edge-based smoothed finite element method on geometrically non-linear plates of non-linear material. European Congress on Computational Methods in Applied Sciences and Engineering (ECCOMAS), Austria, (2012).
- [11] Yao, J., Liu, G.R., Narmoneva D.A., Hinton, R.B. and Zhang, Z.Q. Immersed smoothed finite element method for fluid-structure interaction simulation of aortic valves. *Comput Mech.* (2012) **50**:789-804.
- [12] Bathe, K.J. *Finite Element Procedures.* MIT Press, Prentice-Hall, (1996).
- [13] Duong, M.T., Nguyen, N.H. and Staat, M. Numerical stability enhancement of modeling hyperelastic materials. European Congress on Computational Methods in Applied Sciences and Engineering (ECCOMAS), Austria, (2012).
- [14] Holzapfel, G.A., Gasser T.C. and Ogden, R.W. A new constitutive framework for arterial wall mechanics and a comparative study of material models. *Journal of Elasticity and the Physical Science of Solids.* (2000) **61**:1-48.
- [15] Holzapfel, G.A., Sommer, G., Gasser T.C. and Regitnig, P. Determination of layer-specific mechanical properties of human coronary arteries with nonatherosclerotic intimal thickening and related constitutive modeling. *Am J Physiol Heart Circ Physiol.* (2005) **289**:H2048-58.
- [16] Humphrey, J.D. *Cardiovascular Solid Mechanics-Cells, Tissues, and Organs.* Springer-Verlag, New York, (2002).
- [17] Lubarda, V.A. and Hoger, A. On the mechanics of solids with a growing mass. *International Journal of Solids and Structures.* (2002) **39**:4627-4664.
- [18] Himpel, G., Kuhl E., Menzel A. and Steinmann, P. Computational modelling of isotropic multiplicative growth. *Computer Modeling in Engineering & Sciences.* (2005) **8**:119-134.
- [19] Code Aster. <http://www.code-aster.org>.